Challenges and Opportunities for Next-Generation Manufacturing in Space

Kip Nieman * **A. F. Leonard** * **Katie Tyrrell** *
Dominic Messina * **Rebecca Lopez** * **Helen Durand** *

* *Department of Chemical Engineering and Materials Science, Wayne State University, Detroit, MI 48202 USA (corresponding contact e-mail: helen.durand@wayne.edu).*

Abstract: With commercial space travel now a reality, the idea that people might spend time on other planets in the future seems to have greater potential. To make this possible, however, there needs to be flexible means for manufacturing in space to enable tooling or resources to be created when needed to handle unexpected situations. Next-generation manufacturing paradigms offer significant potential for the kind of flexibility that might be needed; however, they can result in increases in computation time compared to traditional control methods that could make many of the computing resources already available on earth attractive for use. Furthermore, resilience is a significant focus of next-generation manufacturing strategies, and one way to enable resilience for space manufacturing would be to have backup controllers available on earth. These types of considerations raise questions about remote control and monitoring, as well as privacy of the data involved in such practices, that must be considered. This work provides a perspective on several topics tied to remote control and monitoring for manufacturing in space.

Keywords: space manufacturing, next-generation manufacturing, model predictive control, interpretability, cryptography

1 Introduction

Travel or long-term habitation on the surface of Mars and other distant locations in space involves establishing safe living conditions on the order of hundreds of millions of miles from Earth. These distances mean that supplies could take months to reach a space settlement, representing a huge reliability and logistics challenge and making it impossible to rely solely on Earth-based resources. The distances also imply a challenge in aborting missions when emergencies or unexpected events occur, which necessitates increased adaptability and self-sufficiency. Additionally, the significant energy required to transport cargo into near-Earth orbit and the transport time to reach distant settlements will lead to increased (and perhaps prohibitive) mission expenses Owens and de Weck (2016).

Point-of-use manufacturing offers the ability to address many of these issues. Due to its inherent flexibility and small footprint, additive manufacturing is appealing for this purpose, allowing for on-site production in space and avoiding the need to anticipate supply requirements in advance (some of which may not be used in actuality). However, advanced manufacturing in space may require significant computing capabilities. The remoteness of space means that delivering computing equipment to on-site locations may increase shipping expenses, and it may be more difficult to "back-up" information which could pose a challenge for continued operation of key manufacturing processes. For these reasons communication with Earth-based computers, which could function either continuously for control of space-based manufacturing, or be used as back-up in the case of emergencies, is an important consideration and introduces additional challenges. Some issues, such as maintaining privacy of process simulations and monitoring a process remotely, are not specific to space manufacturing, but take on additional importance for space-based resources due to the remoteness of space manufacturing applications (limiting back-up solutions). Furthermore, some challenges, such as large communication delays due to the vast distances that information needs to travel through space, are unique to space manufacturing. In the case of Earth-Mars communication, these delays can add up to a round-trip total of 42 minutes Attwood (2018) and introduce an obstacle to the use of earth-based control actions. Since controllers deal with time-sensitive information, they may struggle to manage processes effectively unless these issues are explicitly considered. This work provides perspectives on several such issues for next-generation manufacturing in space.

2 Motivating Example: Powder Bed Fusion Simulation

In this work, we hypothesize that one step toward safety certification of commercial space travel will include the ability to perform manufacturing in space to obtain needed tooling or materials on demand, and that part of the certification process will require the use of Earth-based computing and control systems as backup or primary systems to provide greater access to resources for remotely handling digital twin computational resources, or control system failure or upgrades. If, for example, additive manufacturing is used as part of this space manufacturing strategy, then because the parts to be created in space would

change regularly, aspects of the manufacturing strategy (including how the process is to be controlled) must also be regularly re-specified. Because space resources are likely to be limited, it would be preferable to reduce the uncertainty in what the necessary operating parameters are to achieve a desired outcome. One idea for seeking to accomplish this is to utilize a digital twin. However, developing a full digital twin of an additive manufacturing process can be complex, requiring many phenomena to be considered, including phase transitions, fluid and solid mechanics, heat transfer, and changes in microstructure. In this section, we use a simplified finite element analysis model of a powder bed fusion (PBF) system (a type of additive manufacturing process) that is designed with consideration of heat conduction, surface convection, and the changing material properties of different phases. Given that PBF is a complex process, some phenomena are neglected, such as fluid and solid mechanics, microstructure changes, convection in the molten metal, radiation, the effects of alloying on melting temperature, wetting, sintering, and gravity in space. Despite the simplicity of the simulation compared to a full PBF system, this simulation still serves to motivate several key issues for space manufacturing that will be discussed in the remainder of this work.

PBF can be used to create metallic components by using a laser to melt successive layers in a bed of metal powder. Each subsequent layer is created by applying a thin layer of powder over the bed and the previously melted section, using a rolling or sweeping mechanism, and using the laser to melt the next layer into the previous. Parts created using PBF are either directly fused to a metal base plate, or supporting structures are added and later removed when finishing the part Mani et al. (2017).

To develop the PBF simulation used as a motivating study, modeling strategies from previous works were synthesized Hussein et al. (2013); Zeng et al. (2015); Goldak et al. (1984) to create an ANSYS thermal simulation of a 0.4 mm by 0.8 mm by 2.75 mm rectangular geometry. The top 80 μm is set as the powder layer, meaning the entire geometry represents a thickness of 5 layers. Custom ANSYS Parametric Design Language (APDL) code command blocks were inserted to include additional functionality. This includes the application of a moving Gaussian volumetric thermal profile applied as heat generation to represent the laser, taken from Goldak et al. (1984):

$$q(\zeta, y, z) = \frac{6\sqrt{3}Q}{R^3\pi\sqrt{\pi}} e^{-3y^2/R^2} e^{-3z^2/R^2} e^{-3\zeta^2/R^2} \quad (1)$$

This equation assumes a laser with power Q and characteristic radius R that moves in the $x-$direction at velocity v. The applied volumetric heat generation q is a function of coordinates y and z and $\zeta = x + v(t - \tau)$, which itself is a function of coordinate x and time t. The τ parameter is used to indicate the laser starting point. The simulations in this work use $Q = 400$ W, $R = 0.00025$ m, $v = 1$ m/s, and $\tau = 0$. Additionally, an absorptivity of 0.8 was assumed, which is applied as a scalar multiple of q in Eq. 1.

The powder bed and base plate were simulated as 316 stainless steel with nonlinear temperature-dependent material properties. Values of the solid-phase specific heat can be found in Deng and Kiyoshima (2010) and the molten-phase in Fukuyama et al. (2019). Density, enthalpy, and thermal conductivity of both the solid and liquid can be found in Mills (2002). To estimate the values of the specific heat, density, enthalpy, and thermal conductivity of the powder, the following equation was applied:

$$M_{powder} = M_{solid}(1 - \phi) \quad (2)$$

M_{powder} and M_{solid} represent a material property (specific heat, density, enthalpy, or thermal conductivity) of the powder and solid phase respectively, and ϕ represents the porosity of the powder phase, assumed to be 0.4. This relation assumes that the value of a property is proportional to the solid fraction of the material, which has been applied in previous studies Hussein et al. (2013); Luo and Zhao (2018). Similar to previous studies, radiation effects were neglected because they are smaller in magnitude when compared to other heat transfer methods (e.g., conduction) Zeng et al. (2015).

The geometry is set to an initial temperature of 300 K, the surface of the powder is subjected to a convection boundary condition with a convection coefficient of 10 $W/m^2/K$, and the underside and sides of the geometry are held at 300 K. During the thermal analysis at the beginning of each time step, custom APDL code manages material properties based on the current phase of the material (powder, liquid, or solid). To accomplish this, two materials were created. One material represents the powder phase and the other the solid phase, and both materials contain material property data for the liquid phase. This means that either phase can be melted without reassigning the material for a particular element. At the end of each load step, a section of the code loops over the nodes in the geometry and selects those which have reached the melting point. The elements attached to these nodes are then assigned to the solid phase. The result is a method of managing the phases to represent the system.

Mesh and time step independence analysis was performed to show how the simulation results depend on the size of the elements or time steps. Table 1 lists the simulation time for six simulations with differing element sizes and/or time step sizes. These simulations were performed on a Z240 Workstation desktop with Windows 10 (Build: 18363), an Intel(R) Xeon(R) CPU E3-1240 v5 @ 3.50GHz processor, 4 cores, and 32 GB RAM. These simulations were not optimized for simulation speed, so the simulation times are for demonstration purposes. Fig 4 shows one of the plots of temperature versus time that was used to analyze mesh and time step independence. The simulation with 40 μm element and 25 μs time steps appears to have an adequate temperature profile, as the results for decreasing the element size to 20 μm led to a maximum percent change of 5.61% and decreasing the time step size to 10 μs led to a maximum percent change of 6.75%.

Table 1. Simulation Information.

Element size (μm)	Time Step size (μs)	Simulated time (μs)	Time to simulate (s)	μs Simulated per Real-Time Second
80	100	2000	325	6.15385
40	100	2000	7571	0.264166
40	25	1500	21392	0.0701197
40	10	2000	65711	0.0304363
20	100	2000	57843	0.0345764
20	25	1500	148293	0.0101151

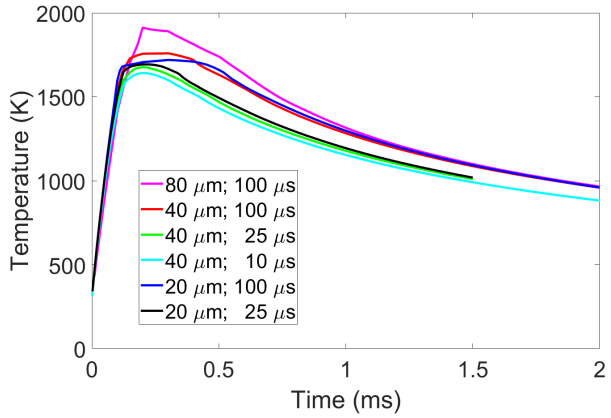

Fig. 1. Temperature vs time plot at the surface of the geometry at $(x, y) = (0, 0)$

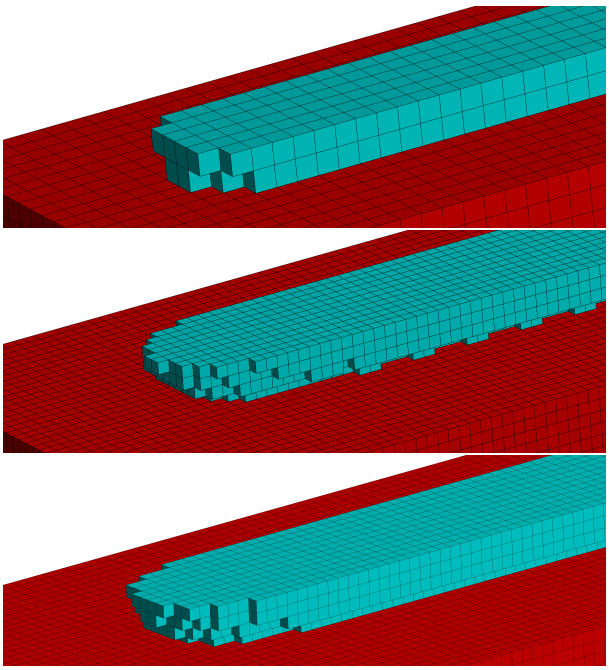

Fig. 2. Resulting solid elements in the $40\mu m$, $25\mu s$ (top), $20\mu m$, $100\mu s$ (middle), and $20\mu m$, $25\mu s$ (bottom) simulation cases.

The elements that reach the melting point (which become part of the completed object) are shown in blue for three cases in Fig. 2, which helps to demonstrate the interdependence between the mesh and time step sizes and the results in terms of part geometry. Comparing the $40\mu m$, $25\mu s$ case (the top image in Fig. 2) to the other two figures, which consist of the smaller $20\mu m$ elements, it can be seen that some resolution is lost when capturing the solid geometry due to the size of each element. This is a consequence of how in ANSYS, each element is assigned one material type and therefore the boundary between the solid metal and the powder must be represented as the surface faces of elements. Additionally, the effects of differing time step sizes can be seen on the bottom two images, which both use elements of size $20\mu m$ but have differing time step sizes of $100\mu s$ (middle image in Fig. 2) and $25\mu s$ (the bottom image in Fig. 2) . The $100\mu s$ simulation has a different resulting solid geometry than the $25\mu s$ simulation, especially near the outer portions of the solid part, which is due to slight differences in temperature. This is caused due to the way that the APDL code assigns materials based on melting point, where the maximum temperature among all of the nodes of each element determines the element's temperature, along with each element being assigned a single material. The elements near the edges of the solid geometry are given a temperature close to the melting point, which means that temperature differences numerically could cause those elements to become solid or remain powder even if the differences in temperature are small. Thus, the selected mesh and time step has a significant effect on the geometry of the completed part and proper independence testing is critical to obtaining correct part geometries.

From the results just described, we can make several observations that motivate the subsequent discussions regarding manufacturing in space: 1) Predicting the outcome of the simplified process simulation required hours of computation time with an adequate mesh and time step in Table 1 and Fig. 2 on the desktop computer used. A full digital twin would be expected to take longer or require higher-performance computers, so that the use of earth-based computing resources (e.g., the Cloud) may be desirable for performing computations related to the manufacturing system. Privacy of the data on the shared computing resource would then be an important consideration. 2) Many phenomena that might be observed in a real PBF process are not included in this simulation; it would be expected that even if additional phenomena were accounted for, it may be a challenge to develop a fully accurate digital twin for a space manufacturing process and to keep it up-to-date at all times. There may be a reduced number of manufacturing experts in space compared to on earth, so that it may be desirable to have means for diagnosing why plant data obtained remotely does not match predictions from a digital twin. 3) The PBF process in the simulation occurs very fast (Table 1), which would make effective earth-based feedback control more difficult. One might consider the trade-offs of running it more slowly and using a digital twin to analyze the effects of that; more broadly, one might have interest in analyzing how the dynamics of a space manufacturing system impact the extent to which advanced controllers on earth can be used to supply control actions to space, and how this might impact process design or the selection of control system frameworks for greatest space portability and earth-based backup.

3 Cloud Privacy and Space Manufacturing

As noted above, computations on the Cloud may be a hallmark of space manufacturing, but would also require data privacy to prevent intellectual property theft or exploitation of information on a space system by a cyberattacker. One method that has been explored for privacy in a control context is homomorphic encryption, which can be used to encrypt information, perform mathematical operations on the encrypted data, and decrypt the solutions. This has been studied for control of linear systems (e.g., encrypting proportional-integral-derivative (PID) control Kogiso and Fujita (2015) and model predictive control (MPC) Darup et al. (2018)) considering that data is transferred in an encrypted state and never decrypted on the Cloud to

maintain privacy during calculations. For example, similar to Kogiso and Fujita (2015), consider the system $\dot{x} = x + u$ under proportional control ($u = -kx$), where x represents the process state, u is the process input, and k is the proportional gain. RSA encryption Rivest et al. (1978), which is a homomorphic encryption algorithm that allows for multiplication on encrypted values, is applied to encrypt x and k, calculate kx in the encrypted space, and decrypt the result to find u. Because RSA is for encryption of integers, the state measurement can be scaled up by multiplication by a factor λ and rounding to the nearest integer, and later dividing the input by λ. Rounding to the nearest integer before encryption can contribute to fluctuations around a value offset from the steady-state (Fig. 3).

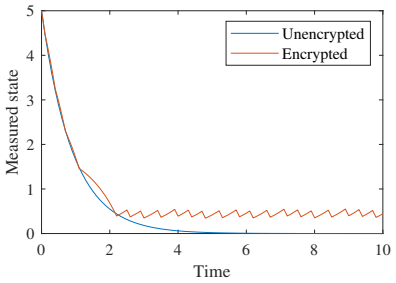

Fig. 3. Encrypted proportional control with $\lambda = 1$.

RSA cannot privately perform addition, which is needed for advanced model-based control (for example, in nonlinear optimization). Attempts to get around this limitation with additional communication between the earth and space systems would suffer from the lengthy communication times involved over large distances. This indicates that constraints tied to the challenges of space manufacturing impact the number of strategies available for ensuring privacy in space manufacturing. Secret sharing is an alternative privacy technique that has been explored (e.g., Darup and Jager (2019)) to divide data (the 'secret') into 'shares' (pieces of the calculation that need to be completed) and are divided among 'shareholders' (separate Cloud computers) to preform calculations. Because only part of the information is available on each Cloud, each individual Cloud lacks the information required to learn the secret. However, if an eavesdropper could gain access to every Cloud, they might learn the secret. Another idea could be to obscure where the calculations are performed (for example, including several decoy Cloud computers performing dummy calculations, such as computing control actions for many different possible state measurements so that an attacker would have to figure out which was the true state measurement, and potentially randomly selecting a Cloud at each time step to receive the correct state measurement). This might aid in slowing an eavesdropper from learning about a process, but it creates computational redundancy. Also, states between sampling periods are related via the process model, which may give the eavesdropper clues that aid them in figuring out the plant data. Further work will be needed to develop sustainable space solutions for Cloud computations.

4 Interpretability for Space Manufacturing Analysis

As noted in Section 2, another aspect of developing a space manufacturing strategy is remote monitoring of a process due to the greater degree of process expertise expected on earth compared to space. When plant data from a space system deviates from expected data based on a digital twin, engineers and operators for the process in space may need assistance from earth in diagnosing the cause. This can be understood as a desire for the data received from space to be "interpretable" to those on earth, or somehow to reveal the process physics (when the "correct" physics may not be fully understood, particularly in relatively unexplored environments such as space, so that parameter estimation using a first-principles model may not be sufficient for providing an understanding of what may have happened). In general, however, defining "interpretability" of data can be a challenge, which is increasingly highlighted through black-box data-driven modeling strategies where many definitions of "interpretability" of the models may exist (e.g., Chakraborty et al. (2017)). One could ask whether neural networks, given their flexibility, might be trained so that some indicator (e.g., the weight distribution) may help to show what happened with the underlying process dynamics. Inspired by Wu and Christofides (2019) which developed a recurrent neural network (RNN) model of a continuous stirred tank reactor (CSTR), we can discuss this within the context of a CSTR. The CSTR dynamic model is given by:

$$\begin{aligned} \frac{dC_A}{dt} &= \frac{F}{V}(C_{A,0} - C_A) - k_0 e^{-E_A/RT} C_A^n \\ \frac{dT_A}{dt} &= \frac{F}{V}(T_{A,0} - T_A) - \frac{k_0 e^{-E_A/RT} \Delta H_r}{\rho c_p} C_A^n + \frac{Q_C}{\rho c_p V} \end{aligned} \tag{3}$$

where C_A and T are the reactant concentration and temperature, and the manipulated inputs are the inlet reactant concentration C_{A0} and heat rate input Q. The reaction order is $n = 2$, the reaction rate constant is $k_0 = 8.46 \times 10^6$ $(m^3 kmol^{-1})^{n-1} h^{-1}$, the activation energy is $E_A = 5 \times 10^4$ $kJ/kmol$, and the molar heat of reaction is $\Delta H_r = -1.15 \times 10^4$ $kJ/kmol$. The reaction medium has a density of $\rho = 10^3$ kg/m^3 and specific heat capacity of $c_p = 0.231$ $kJ\ kg^{-1} K^{-1}$. The CSTR was simulated with an integration step of 10^{-4} h, with inputs applied in sample-and-hold with a sampling period of 0.01 h. An RNN was designed to predict the values of C_A and T at the end of 10 integration steps given the state measurements and inputs at the beginning of this time period. It was trained using data from open-loop simulations over a sampling period from a variety of initial states and using a variety of different inputs. 10 integration steps were used for every batch. Keras and Tensorflow were used to generate a neural network consisting of a SimpleRNN with 8 hidden states and a Dense layer with 2 outputs corresponding to C_A and T at the end of 0.001 h. Because 10 data points are available across 0.001 h, these were used in training with the return_sequences = True command and by using the data ($C_A(t_k)$, $T(t_k)$, $C_{A0}(t_k)$, and $Q(t_k)$) for the RNN. The activation functions were chosen as hyperbolic tangents. The full model structure is shown in Table 2. The model was tuned with a 9:1 training and test data split over a single epoch. The RNN was re-trained using data with a reaction order of 1 (Case 1) and with a reaction order of 3 (Case 2). The mean absolute errors for the normalized training data for the Baseline (reaction order 2), Case 1, and Case 2 scenarios were 0.00425, 0.00355, and 0.00380, with the absolute error for the normalized test data at 0.00426, 0.00356, and 0.00381. The weights of the trained neural networks for the three cases were obtained, and

Table 2. Sequential Model Structure: Total number of tuneable parameters = 122

Layer Type	Output Shape	No of parameters
simple_rnn	(None, 10, 8)	104
dense	(None, 10, 2)	18

a heat map was generated showing the differences in the weights of Case 1 and Case 2 with respect to the Baseline case (Fig. 4). There are locations within the maps where weights change significantly between cases, and where they do not; however, a large-scale pattern is not obvious and assessing whether one exists and how it depends on the training data and procedure would require further analysis. Understanding when and how unknown physics might be remotely monitored and diagnosed from earth remains an important challenge for effective space manufacturing.

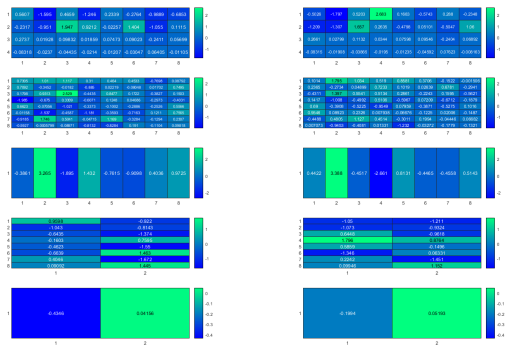

Fig. 4. Weights for Case 1 - Baseline (left) and for Case 2 - Baseline (right) in a heat map. Weight difference values are indicated on the plots. The x-axis indicates layer inputs and the y-axis indicates layer outputs

5 Delayed Measurements in Earth-Based Control

The final challenge for space manufacturing which we address is the significant communication delay. As noted in Section 2, it would be desirable to understand the conditions under which space manufacturing systems can provably handle the communication delay to guide in process design and computing architecture selection for space. In this section, we provide a perspective on this using Lyapunov-based economic model predictive control (LEMPC) for processes designed to operate in a region around an operating steady-state and which can be driven toward it at any point in time. The selection of this control law is due to prior studies investigating LEMPC for processes with measurement delay Heidarinejad et al. (2012) and because of its ability to optimize economics for next-generation manufacturing. LEMPC is a model-based controller that solves an optimization problem at every sampling time. This section updates time delay-handling for LEMPC to consider the space manufacturing-specific consideration of delayed inputs as well as measurements.

5.1 Preliminaries

5.1.1 Notation The notation $|x|$ represents the Euclidean norm and x^T represents the transpose of a vector x. The function $\alpha : [0, a) \to [0, \infty)$ is a class $\mathcal{K}$ function if $\alpha(0) = 0$, and if it is continuous and strictly increasing. For a scalar-valued function $V(x)$, $\Omega_\rho := \{x \in \mathbb{R}^n : V(x) \leq \rho\}$. Set subtraction is denoted using '/' (i.e., $A/B := \{x \in \mathbb{R}^n : x \in A, x \notin B\}$). A sampling time is represented as $t_k := k\Delta, k = 0, 1, 2, ...$, where Δ is the sampling period.

5.1.2 Class of systems In this work, the following class of systems is considered:

$$\dot{x} = f(x(t), u(t), w(t)) \tag{4}$$

where $x \in X \subset \mathbb{R}^n$ is the state vector, $u \in U \subset \mathbb{R}^m$ is the input vector, and $w \in W \subset \mathbb{R}^z$ is the disturbance vector. f is a locally Lipschitz on $X \times U \times W$. W and U are defined as $W := \{w \in \mathbb{R}^z : |w| \leq w^{\max}, w^{\max} > 0\}$ and $U := \{u \in \mathbb{U}^m : |u| \leq u^{\max}\}$. We consider the nominal system ($w \equiv 0$) which is stabilizable through the application of an asymptotically stabilizing feedback control law $h(x)$, a sufficiently smooth Lyapunov function $V(x)$, and class $\mathcal{K}$ functions $\alpha_i(\cdot), i = 1, 2, 3, 4$, where, $\forall x \in D \subset \mathbb{R}^n$ (D is an open neighborhood of the origin):

$$\alpha_1(|x|) \leq V(x) \leq \alpha_2(|x|) \tag{5a}$$

$$\frac{\partial V(x)}{\partial x} f(x, h(x), 0) \leq -\alpha_3(|x|) \tag{5b}$$

$$\left| \frac{\partial V(x)}{\partial x} \right| \leq \alpha_4(|x|) \tag{5c}$$

$$h(x) \in U \tag{5d}$$

Ω_ρ is defined as the stability region of the nominal closed-loop system under the Lyapunov-based controller $h(x)$ and is chosen so that $x \in X, \forall x \in \Omega_\rho$.

5.2 LEMPC Formulation for Space Manufacturing with Earth-based Cloud Resources

The LEMPC formulation incorporating both measurement and input application delay is:

$$\min_{u(t) \in S(\Delta)} \quad \int_{t_k}^{t_k + N\Delta} [l_e(\breve{x}(\tau), u(\tau))] d\tau \tag{6a}$$

$$\text{s.t.} \quad \dot{\breve{x}}(t) = f(\breve{x}(t), u(t), 0) \tag{6b}$$

$$u(t) = u^*(t), t \in [t_k - D, t_k + D) \tag{6c}$$

$$u(t) \in U, t \in [t_k + D, t_k + N\Delta) \tag{6d}$$

$$\breve{x}(t_k - D) = \bar{x}(t_k - D) \tag{6e}$$

$$V(\breve{x}(t)) \leq \rho_e, \quad \forall\, t \in [t_k + D, t_k + N\Delta) \quad \text{if} \quad V(\breve{x}(t_k + D)) \leq \rho_e \tag{6f}$$

$$\frac{\partial V(\breve{x}(t_k + D))}{\partial x} f(\breve{x}(t_k + D), u(t_k + D), 0) \leq \frac{\partial V(\breve{x}(t_k + D))}{\partial x} f(\breve{x}(t_k + D), h(\breve{x}(t_k + D)), 0) \quad \text{if } V(\breve{x}(t_k + D)) > \rho_e \tag{6g}$$

where $\breve{x}$ and u represent the estimated state and optimized input values, respectively. $\bar{x}$ represents the actual state of the process and $u^*(t)$ represents all of the inputs from $t_k - D$ to $t_k + D$. $u(t) \in S(\Delta)$ in equation 6a indicates that $u(t)$ is a piecewise-constant input vector with N sections (N is the length of the prediction horizon), each held for a single sampling period of time length Δ.

The one-way communication delay between Earth and a space manufacturing system (e.g., on Mars) is represented as D, and at each time step, the process state at the

location of the process is $\bar{x}(t_k - D)$ (changes in the delay length time as the earth and Mars orbit about the sun is not considered here for simplicity). The signal is then sent to Earth where it arrives in D time units and is used in the LEMPC as $x(t_k)$. The LEMPC calculates $\breve{x}(t_k)$ and $\breve{x}(t_k + D)$ using a nominal model. The value of $\breve{x}(t_k)$ represents a prediction by the controller on Earth of the process state on Mars at the time of calculation. The controller also needs to predict the state that will exist once the signal travels to Mars, designated as $\breve{x}(t_k + D)$, which is used to calculate the applied control action $u(t_k + D)$. An example of the predictions made by the controller is, assuming a round-trip communication delay of 40 minutes, the model must be able to predict the necessary control actions from 20 minutes into the future using The state measurements from 20 minutes in the past. The control actions that will be applied during this period must also be predicted.

If there is no plant-model mismatch and the predictions made the controller are perfectly accurate, a stabilizing control action for the prediction would also be stabilizing for the process. The controller would then inherit the feasibility and stability theoretical properties from Heidarinejad et al. (2012). However, in realistic cases with plant-model mismatch, additional theoretic study would be required as the actual process dynamics will deviate from those of the model. Particularly in cases where the process dynamics are fast, this would be expected to make it more challenging to control the system with delay from earth unless the plant/model mismatch is very low. Given the possible difficulty of finding accurate process models, methods of ensuring optimal operation with less accurate models, such as potentially sending a set of control actions instead of only a single control action corresponding to various possible state measurements and letting the system on Mars select which is the most applicable at the time of application, could be a beneficial direction for future work.

Acknowledgements

Financial support from the Air Force Office of Scientific Research (award number FA9550-19-1-0059), National Science Foundation CNS-1932026 and CBET-1839675, Michigan Space Grant Research Consortium award numbers NNX15AJ20H and 80NSSC20M0124, Wayne State University Grants Boost funding, and Wayne State University is gratefully acknowledged. We wish to thank Emily Kopmanis, Courtney Felder, Jessica Pikunas, and Olamide Alabi for joining the discussion in learning about neural networks and interpretability.

Literature Cited

Attwood, J.R. (2018). Mars in 2018. *The Journal of The Royal Astronomical Society of Canada*, 112, 121–122.

Chakraborty, S., Tomsett, R., Raghavendra, R., Harborne, D., Alzantot, M., Cerutti, F., Srivastava, M., Preece, A., Julier, S., Rao, R.M., Kelley, T.D., Braines, D., Sensoy, M., Willis, C.J., and Gurram, P. (2017). Interpretability of deep learning models: A survey of results. In *2017 IEEE SmartWorld, Ubiquitous Intelligence & Computing, Advanced & Trusted Computed, Scalable Computing & Communications, Cloud & Big Data Computing, Internet of People, and Smart City Innovation*, 1–6. San Francisco, California.

Darup, M.S. and Jager, T. (2019). Encrypted cloud-based control using secret sharing with one-time pads. In *IEEE Conference on Decision and Control*, 7215–7221. Nice, France.

Darup, M.S., Redder, A., and Quevedo, D.E. (2018). Encrypted cloud-based MPC for linear systems with input constraints. *IFAC-PapersOnLine*, 51, 535–542.

Deng, D. and Kiyoshima, S. (2010). Numerical simulation of residual stresses induced by laser beam welding in a SUS316 stainless steel pipe with considering initial residual stress influences. *Nuclear Engineering and Design*, 240, 688–696.

Fukuyama, H., Higashi, H., and Yamano, H. (2019). Thermophysical properties of molten stainless steel containing 5 mass % B4C. *Nuclear Technology*, 205, 1154–1163.

Goldak, J., Chakravarti, A., and Bibby, M. (1984). A new finite element model for welding heat sources. *Metallurgical Transactions B*, 15, 299–305.

Heidarinejad, M., Liu, J., and Christofides, P.D. (2012). Economic model predictive control of nonlinear process systems using Lyapunov techniques. *AIChE Journal*, 58(3), 855–870.

Hussein, A., Hao, L., Yan, C., and Everson, R. (2013). Finite element simulation of the temperature and stress fields in single layers built without-support in selective laser melting. *Materials Design (1980-2015)*, 52, 638–647.

Kogiso, K. and Fujita, T. (2015). Cyber-security enhancement of networked control systems using homomorphic encryption. In *IEEE Conference on Decision and Control*, 6836–6843. Osaka, Japan.

Luo, Z. and Zhao, Y. (2018). A survey of finite element analysis of temperature and thermal stress fields in powder bed fusion additive manufacturing. *Additive Manufacturing*, 21, 318–332.

Mani, M., Lane, B.M., Donmez, M.A., Feng, S.C., and Moylan, S.P. (2017). A review on measurement science needs for real-time control of additive manufacturing metal powder bed fusion processes. *International Journal of Production Research*, 55, 1400–1418.

Mills, K. (2002). *Recommended Values of Thermophysical Properties for Selected Commercial Alloys*. Woodhead Publishing.

Owens, A. and de Weck, O. (2016). Systems analysis of in-space manufacturing applications for the international space station and the evolvable Mars campaign. In *AIAA SPACE 2016*, 5394.

Rivest, R., Shamir, A., and Adleman, L. (1978). A method for obtaining digital signatures and public-key cryptosystems. *Communications of the ACM*, 21, 120–126.

Wu, Z. and Christofides, P.D. (2019). Economic machine-learning-based predictive control of nonlinear systems. *Mathematics*, 7, 494.

Zeng, K., Pal, D., Gong, H., Patil, N., and Stucker, B. (2015). Comparison of 3dsim thermal modelling of selective laser melting using new dynamic meshing method to ansys. *Materials Science and Technology*, 31, 945–956.